Hybrid Observer Concept for Sensor Fusion of Sporadic Measurements for Underwater Navigation *

Jens E. Bremnes[1], Astrid H. Brodtkorb[1], Asgeir J. Sørensen[1]

[1]Department of Marine Technology (IMT), Norwegian University of Science and Technology (NTNU), Norway Centre for Autonomous Marine Operations and Systems (AMOS)
Emails: {jens.e.bremnes, astrid.h.brodtkorb, asgeir.sorensen}@ntnu.no

Abstract

Accurate underwater navigation systems are required for closed-loop guidance and control of unmanned underwater vehicles (UUV). This paper proposes a sensor-based hybrid translational observer concept for underwater navigation using the hybrid dynamical systems framework, accounting for noisy, asynchronous and sporadic sensor measurements. Sensor measurements from an acoustic positioning system, a Doppler Velocity Log (DVL), an Inertial Measurement Unit (IMU) and a pressure gauge are used in the proposed observer. A method for filtering high-frequency noise is proposed, where the estimated states are obtained by taking a weighted discounted average of a finite number of previous measurements predicted forwards to the current time. The attitude of the vehicle is assumed known, and the acceleration measurements are assumed to be continuously available. Measurements of position, depth and linear velocity are assumed to be asynchronous and sporadically available, that is, they do not arrive at the same time, and their sampling rates are not constant. Uniform global asymptotic stability (UGAS) is established using Lyapunov theory for hybrid systems. Results from simulations are presented in order to demonstrate the performance of the proposed method.

1 Introduction

Accurate underwater navigation systems are required for closed-loop guidance and control of UUVs. [1] gives an overview of several underwater navigation

*This work was supported by the Research Council of Norway through the Centre of Excellence funding scheme, NTNU AMOS, project number 223254, and the UNLOCK project, through the Research Council of Norway FRINATEK funding scheme, project number 274441.

techniques. Many UUVs today use model-based observers. By including a kinetic model of the vehicle, these observers are able to filter out noise, reconstruct unmeasured states, estimate biases, and in the case of signal loss, do dead reckoning. [2] propose a Kalman filter for Remotely Operated Vehicles (ROV). Drawbacks of Kalman filters are the large number of parameters to be tuned, and the unproved mathematical stability proofs for certain applications, such as global stability results for extended Kalman filters. On the contrary, nonlinear passive filters are able to provide proof of global stability. [3] propose a model-based nonlinear Luenberger observer using the observer backstepping technique, which proved to be UGAS. A shortcoming of model-based observers is that the bias estimate is not able to capture rapidly changing loads and environmental conditions. Hence, regarding tuning, there is a trade-off between performance during steady-state conditions and transients.

Sensor-based observers on the other hand, often called a strap-down approach, rely purely on the sensor measurements and kinematic relationships. Thus, all unknown forces acting on the vehicle are captured in the observer instantaneously by the accelerometers. In [4] a sensor-based integration filter for the estimation of translational motion of UUVs is proposed. A drawback of strap-down approaches is that these solutions are sensitive to the accuracy of the attitude estimation relying on the sensor measurements only, and in the case of signal loss, they are not able to predict the states in a satisfying manner. Good models of the gravity and centripetal accelerations are also required. Most approaches to observer design assume that sensor measurements are continuously available, or that the sampling rates remain constant.

This paper is a continuation of the authors' previous work in [5]. Here, a method for the design of a sensor-based translational observer using the framework of hybrid dynamical systems [6] applied to UUVs, accounting for noisy, asynchronous and sporadically available sensor measurements was developed. The approach for combining measurements of different fidelities is inspired by [7]. The attitude of the UUV is assumed known, and the acceleration measurements are assumed to be continuously available. The observer is modeled as a cascaded system of three hybrid observers, where acceleration measurements and velocity estimates are continuously integrated in order to obtain velocity and position predictions, respectively, corrected by occasional discrete measurement updates. Each hybrid observer keeps a finite number of the most recent measurements, predicted forward to the current time using the flow dynamics. A method for filtering high-frequency measurement noise is proposed, where the position and velocity estimates are obtained by taking a weighted discounted average of the observer states, giving higher trust to more recent predictions. A new result of this paper is the stability analysis for hybrid cascaded systems proving the observer uniformly asymptotically stable (UGAS). Also, results from simulations in closed-loop with a kinetic vehicle model and control systems are presented to demonstrate the performance of the proposed method.

The paper is organized as follows: In Section 2, the kinematic equations of the observer are presented, as well as the hybrid dynamical systems framework. The observer design is proposed in Section 3, with stability analysis in Section

4. The observer is tested in simulations using MATLAB/Simulink in Section 5. Section 6 concludes the paper.

2 Mathematical modeling

2.1 Kinematics of an underwater vehicle

The 6 degrees-of-freedom (DOF) equation of motion for an underwater vehicle is expressed by the Earth-fixed position vector $\boldsymbol{\eta} = [\boldsymbol{p}^\top \quad \boldsymbol{\Theta}^\top]^\top = [N\ E\ D\ \phi\ \theta\ \psi]^\top \in \mathbb{R}^6$ and the body-fixed velocity vector $\boldsymbol{\nu} = [\boldsymbol{v}^\top\ \boldsymbol{\omega}^\top]^\top = [u\ v\ w\ p\ q\ r]^\top \in \mathbb{R}^6$, where the three first elements in the vectors correspond to the linear part of the motion, and the three latter elements correspond to the angular part of the motion. The sensor-based translational observer is based on the kinematic relationship between the Earth-fixed linear velocities $\dot{\boldsymbol{p}}$, the body-fixed linear velocities $\boldsymbol{v}$ and the body-fixed linear accelerations $\boldsymbol{a}$ through the transformation

$$\begin{aligned} \dot{\boldsymbol{p}} &= \boldsymbol{R}(\boldsymbol{\Theta})\boldsymbol{v} \\ \dot{\boldsymbol{v}} &= \boldsymbol{a} \end{aligned} \tag{1}$$

where $\boldsymbol{R}(\boldsymbol{\Theta})$ denotes the Euler angle transformation given by

$$\boldsymbol{R}(\boldsymbol{\Theta}) = \begin{bmatrix} c\psi c\theta & -s\psi c\phi + c\psi s\theta s\phi & s\psi s\phi + c\psi c\theta s\phi \\ s\psi c\theta & c\psi c\phi + s\phi s\theta s\psi & -c\psi s\phi + s\theta s\psi c\phi \\ -s\theta & c\theta s\phi & c\theta c\phi \end{bmatrix}$$

and $s\,\cdot = \sin(\cdot)$, $c\,\cdot = \cos(\cdot)$ and $t\,\cdot = \tan(\cdot)$.

2.2 Measurements

UUVs typically navigate using four different sensors taking measurements at different sampling rates: Inertial Measurement Units (IMU), Doppler Velocity Logs (DVL), pressure gauges and hydroacoustic transponders [8]. IMUs include accelerometers for linear acceleration measurements and gyroscopes for angular velocity measurements at a sampling rate of $100 - 200$ Hz. DVLs are used to measure linear velocities and altitude at a sampling rate of $0.5 - 5$ Hz. Pressure gauges measure depth with a sampling rate of $0.8 - 8$ Hz. Transponders, part of an acoustic positioning system, measure position relative to a transducer with a sampling rate of $0.2 - 2$ Hz.

In the observer design and analysis, it is assumed that the sensor measurements do not contain any noise or biases, such that they represent the true states of the system. However, in the numerical simulations, noise is added on all sensor measurements. The position, depth and velocity measurements are obtained with a non-constant sample time in the interval $[\underline{T}_m, \overline{T}_m]$ with Gaussian distributed noise with variance σ_m^2 for $m \in \{1, 2, 3\}$, where the index $m = 1$ represents acoustic positioning measurements, $m = 2$ represents pressure gauge

depth measurements, and $m = 3$ represents DVL velocity measurements. Gaussian distributed noise with variance σ_{imu}^2 is added to the acceleration measurements, which are assumed continuously available. Furthermore, it is assumed that the vehicle's attitude $\boldsymbol{\Theta}$ is known.

Note that the depth may be measured by both the acoustic positioning system and the pressure gauge. Since the pressure gauge provides depth measurements with higher accuracy and sampling rate than the acoustic positioning system, we utilize these measurements only when estimating the depth.

2.3 Hybrid Dynamical Systems

The hybrid dynamical system framework presented in [6] can be used to model and analyze systems with both continuous and discrete dynamics. In general, a hybrid system $\mathcal{H}$ can be modeled as

$$\mathcal{H} = \begin{cases} \boldsymbol{x} \in C & \dot{\boldsymbol{x}} \in \boldsymbol{F}(\boldsymbol{x}) \\ \boldsymbol{x} \in D & \boldsymbol{x}^+ \in \boldsymbol{G}(\boldsymbol{x}) \end{cases} \tag{2}$$

where $\boldsymbol{x}$ is the state vector, $C \subset \mathbb{R}^n$ is the flow set, $\boldsymbol{F} : \mathbb{R}^n \rightrightarrows \mathbb{R}^n$ is the flow map, $D \subset \mathbb{R}^n$ is the jump set and $\boldsymbol{G} : \mathbb{R}^n \times \mathbb{R}^m \rightrightarrows \mathbb{R}^n$ is the jump map.

For more information regarding hybrid dynamical systems, the reader is referred to [6].

3 Hybrid observer design

A method for the design of a cascaded sensor-based hybrid translational observer $\mathcal{H}$ consisting of a hybrid velocity sub-system $\mathcal{H}_3$ in cascade with two other hybrid position and depth sub-systems $\mathcal{H}_1$ and $\mathcal{H}_2$ respectively, is proposed. A block diagram of the cascaded hybrid observer structure is shown in Figure 1.

For convenience, we split the translational position $\boldsymbol{p}$ into two components: the horizontal-plane position $\boldsymbol{\xi} \triangleq [N\ E]$ (measured by the acoustic positioning system) and the depth $z \triangleq D$ (measured by the pressure gauge). Furthermore, we constrain the positions and the velocities to a compact set $\mathcal{K} \subset \mathbb{R}^6$ such that $(\boldsymbol{\xi}, z, \boldsymbol{v}) \in \mathcal{K}$. The observer design does not depend on this set.

3.1 Mathematical formulation of the hybrid observer

Each observer has N_m observer states, denoted $(\cdot)_n$ for $n \in \{1, ..., N_m\}$, $m \in \{1, 2, 3\}$, representing copies of position, depth and velocity measurements predicted forwards to the current time using the flow dynamics by integration. The observer states work as a first-in-first-out (FIFO) queue (shift register). New measurements are stored in the first observer state $(\cdot)_1$, while the remainder of the states are shifted one place back. The last observer state $(\cdot)_{N_m}$ with the most outdated prediction is pushed out of the queue and deleted. The time before a new measurement is randomly selected from an interval $[\underline{T}_m, \overline{T}_m]$,

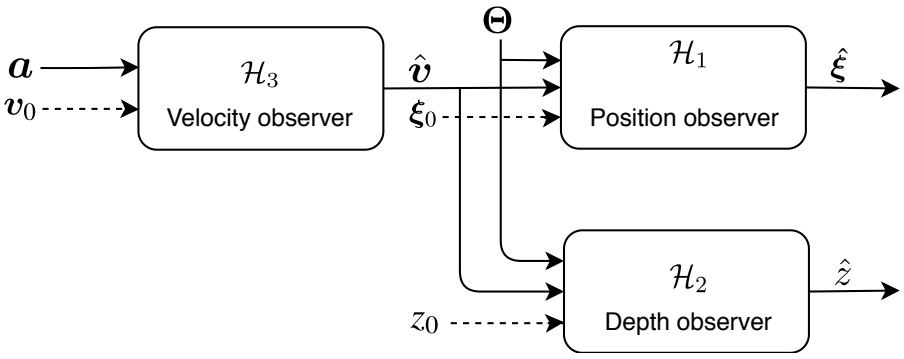

Figure 1: Block diagram showing the cascade structure of the hybrid observer. Solid lines denote input to the flow dynamics, and dashed lines denote input to the jump dynamics.

where $\underline{T}_m$ and $\overline{T}_m$ represent the lower and upper bounds for the sampling time characterized by sensor m, respectively.

For filtering high-frequency noise, a method inspired by a weighting scheme in [9] is proposed. The observer estimates are obtained by taking a weighted discounted average of the observer states, given by

$$\hat{\boldsymbol{\xi}} := \frac{\sum_{i=1}^{N_1} \gamma_1^i \boldsymbol{\xi}_i}{\sum_{i=1}^{N_1} \gamma_1^i}, \quad \hat{z} := \frac{\sum_{j=1}^{N_2} \gamma_2^j z_j}{\sum_{j=1}^{N_2} \gamma_2^j}, \quad \hat{\boldsymbol{v}} := \frac{\sum_{k=1}^{N_3} \gamma_3^k \boldsymbol{v}_k}{\sum_{k=1}^{N_3} \gamma_3^k} \tag{3}$$

where $\gamma_m \in (0, 1]$, $m \in \{1, 2, 3\}$, is a constant discount factor, and $\boldsymbol{\xi}_i$, z_j and $\boldsymbol{v}_k$ are the i^{th} position, j^{th} depth and k^{th} velocity states, respectively. The motivation for using a weighted discounted average is that we may have a higher trust in more recent predictions, as these states have integrated possible errors for a shorter time. Note that when $\gamma_m = 1$, we get the mean value of the observer states. In Figure 2, an example of a time series of the evolution of the observer states in the position observer with $N_1 = 3$ is shown. A large variance and a constant sampling rate of $T_1 = 5$ seconds on the position measurement was included for better visualization. The first observer state is here initialized at the true position.

In the velocity observer $\mathcal{H}_3$, the dynamics flow with the acceleration measurements in between the velocity measurements - that is, when $\tau_3 \in [0, \overline{T}_3]$. The observer states are then updated discretely when new velocity measurements are available. The counter variable τ_3 counts backwards in time, such that jumps are triggered when $\tau_3 = 0$. The velocity observer is, for $k \in \{1, ..., N_3\}$, given by

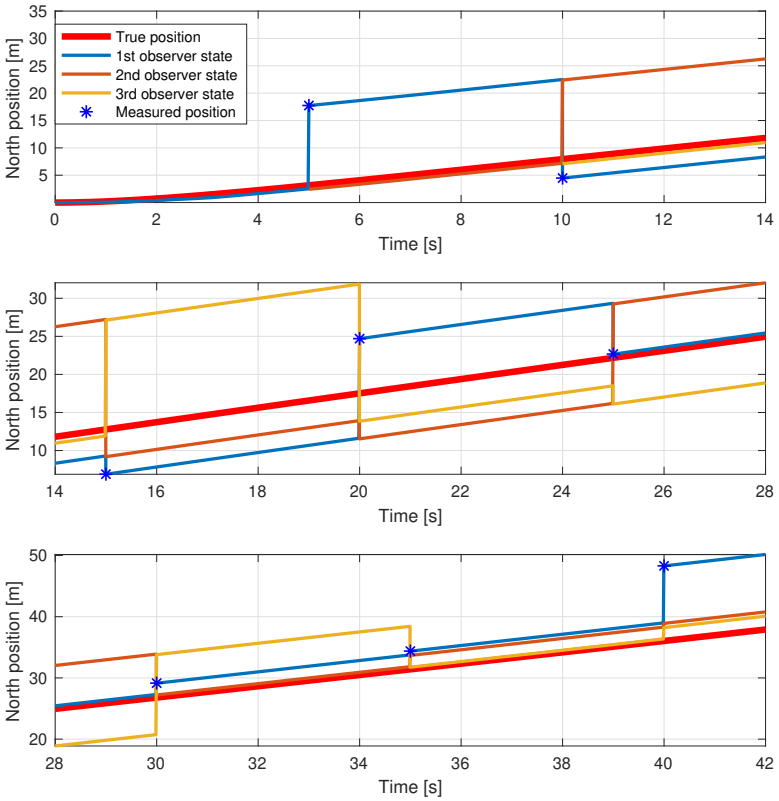

Figure 2: Time series of the evolution of the North position observer states with $N_1 = 3$. The estimated position at a given time is found by taking the weighted discounted average of the three observer states.

$$\mathcal{H}_3 := \begin{cases} \dot{\boldsymbol{v}}_k & = \boldsymbol{a} \\ \dot{\tau}_3 & = -1 \end{cases} \Bigg\} (\boldsymbol{v}_k, \tau_3) \in \mathbb{R}^3 \times [0, \overline{T}_3] \\ \begin{cases} \boldsymbol{v}_k^+ & = \boldsymbol{v}_{k-1} \\ \tau_3^+ & \in [\underline{T}_3, \overline{T}_3] \end{cases} \Bigg\} (\boldsymbol{v}_k, \tau_3) \in \mathbb{R}^3 \times \{0\} \tag{4}$$

where $\boldsymbol{v}_0$ is the DVL linear velocity measurement.

In the position observer $\mathcal{H}_1$, the position states $\boldsymbol{\xi}_i$ flow with the velocity estimate in (3), and are similarly updated discretely when new position measurements are available. The position observer is, for $i \in \{1, ..., N_1\}$, given by

$$\mathcal{H}_1 := \begin{cases} \dot{\boldsymbol{\xi}}_i & = \boldsymbol{I}_{1:2} \boldsymbol{R}(\boldsymbol{\Theta}) \hat{\boldsymbol{v}} \\ \dot{\tau}_1 & = -1 \end{cases} \Bigg\} (\boldsymbol{\xi}_i, \tau_1) \in \mathbb{R}^2 \times [0, \overline{T}_1] \\ \begin{cases} \boldsymbol{\xi}_i^+ & = \boldsymbol{\xi}_{i-1} \\ \tau_1^+ & \in [\underline{T}_1, \overline{T}_1] \end{cases} \Bigg\} (\boldsymbol{\xi}_i, \tau_1) \in \mathbb{R}^2 \times \{0\} \tag{5}$$

where $\boldsymbol{\xi}_0$ is the acoustic position measurement, and

$\boldsymbol{I}_{1:2} := \begin{bmatrix} 1 & 0 & 0 \\ 0 & 1 & 0 \end{bmatrix}$.

The depth observer $\mathcal{H}_2$ is, for $j \in \{1, ..., N_2\}$, given by

$$\mathcal{H}_2 := \begin{cases} \dot{z}_j & = \boldsymbol{I}_3 \boldsymbol{R}(\boldsymbol{\Theta}) \hat{\boldsymbol{v}} \\ \dot{\tau}_2 & = -1 \end{cases} \Bigg\} (z_j, \tau_2) \in \mathbb{R} \times [0, \overline{T}_2] \\ \begin{cases} z_j^+ & = z_{j-1} \\ \tau_2^+ & \in [\underline{T}_2, \overline{T}_2] \end{cases} \Bigg\} (z_j, \tau_2) \in \mathbb{R} \times \{0\} \tag{6}$$

where z_0 is the pressure gauge depth measurement, and $\boldsymbol{I}_3 := [0\ 0\ 1]$.

4 Stability analysis

The compact set for which we are analyzing stability is

$$\begin{aligned} \mathcal{A} := \{ & \boldsymbol{\xi}, z, \boldsymbol{v}, \boldsymbol{\xi}_i, z_j, \boldsymbol{v}_k, \tau_1, \tau_2, \tau_3 \in C : \\ & \boldsymbol{\xi}_i = \boldsymbol{\xi},\ z_j = z,\ \boldsymbol{v}_k = \boldsymbol{v},\ \forall i \in \{1, ..., N_1\}, \\ & \forall j \in \{1, ..., N_2\},\ \forall k \in \{1, ..., N_3\} \} \end{aligned} \tag{7}$$

where

$$C := \mathcal{K} \times \mathbb{R}^{2N_1 + N_2 + 3N_3} \times [0, \overline{T_1}] \times [0, \overline{T_2}] \times [0, \overline{T_3}] \tag{8}$$

We are using Lyapunov results for hybrid systems [6] and cascaded systems [10] to prove that the cascaded observer dynamics given in (4), (5) and (6) has the set $\mathcal{A}$ uniformly globally asymptotically stable (UGAS).

Theorem 1: The set $\mathcal{A}$ in (7) is UGAS for the cascaded hybrid system consisting of the plant (1), and the hybrid sub-systems (4), (5) and (6). □

The proof is done sequentially in several steps in the next Sections. The error dynamics of the observer are given. Firstly, the velocity error dynamics are shown UGAS. Secondly, the position observer error dynamics are shown UGAS under the assumption that the estimated velocity is equal to the true velocity. Thirdly, the cascaded system consisting of the velocity observer and the position observer with a non-zero velocity estimation error is proved UGAS using cascade theory. This is done by proving the position observer error dynamics input-to-state stable (ISS) in two steps; by first looking at the case when $N_1 = 1$, and then at the case when $N_1 > 1$ for $i \in \{2, ..., N_1\}$. Using the same procedure, it follows that the cascaded system consisting of the velocity observer and the depth observer is UGAS.

4.1 Error dynamics

We define the error coordinates as

$$\begin{aligned} \tilde{\boldsymbol{\xi}}_i &:= \boldsymbol{\xi}_i - \boldsymbol{\xi}_{i-1}, \quad && \forall i \in \{1, ..., N_1\} \\ \tilde{z}_j &:= z_j - z_{j-1}, \quad && \forall j \in \{1, ..., N_2\} \\ \tilde{\boldsymbol{v}}_k &:= \boldsymbol{v}_k - \boldsymbol{v}_{k-1}, \quad && \forall k \in \{1, ..., N_3\} \end{aligned} \tag{9}$$

where $\tilde{\boldsymbol{\xi}}_0 := \mathbf{0}$, $\tilde{z}_0 := 0$ and $\tilde{\boldsymbol{v}}_0 := \mathbf{0}$.

The velocity error dynamics are independent of the position and depth error dynamics, and the velocity estimates are input to the position and depth error dynamics. Thus, the total observer error dynamics has a cascaded structure, where the velocity error dynamics are given by

$$\begin{aligned} \dot{\tilde{\boldsymbol{v}}}_k &= \mathbf{0} && k \in \{1, ..., N_3\} \\ \dot{\tau}_3 &= -1 \\ \tilde{\boldsymbol{v}}_k^+ &= \tilde{\boldsymbol{v}}_{k-1} && k \in \{1, ..., N_3\} \\ \tau_3^+ &\in [\underline{T}_3, \overline{T}_3] \end{aligned} \tag{10}$$

and the position and depth error dynamics by

$$
\begin{aligned}
\dot{\tilde{\boldsymbol{\xi}}}_i &= \begin{cases} \boldsymbol{I}_{1:2}\boldsymbol{R}(\boldsymbol{\Theta})(\hat{\boldsymbol{v}} - \boldsymbol{v}) & i = 1 \\ \boldsymbol{0} & i \in \{2, ..., N_1\} \end{cases} \\
\dot{\tilde{z}}_j &= \begin{cases} \boldsymbol{I}_3\boldsymbol{R}(\boldsymbol{\Theta})(\hat{\boldsymbol{v}} - \boldsymbol{v}) & j = 1 \\ 0 & j \in \{2, ..., N_2\} \end{cases} \\
\dot{\tau}_1 &= -1 \\
\dot{\tau}_2 &= -1 \\
\tilde{\boldsymbol{\xi}}_i^+ &= \tilde{\boldsymbol{\xi}}_{i-1} \qquad i \in \{1, ..., N_1\} \\
\tilde{z}_j^+ &= \tilde{z}_{j-1} \qquad j \in \{1, ..., N_2\} \\
\tau_1^+ &\in [\underline{T}_1, \overline{T}_1] \\
\tau_2^+ &\in [\underline{T}_2, \overline{T}_2]
\end{aligned}
\tag{11}
$$

4.2 Velocity error analysis

We start by analyzing the stability of the velocity observer $\mathcal{H}_3$, as its output is input to the sub-systems $\mathcal{H}_1$ and $\mathcal{H}_2$.

Claim 1: The origin of the velocity error dynamics in (10) with states $\tilde{\boldsymbol{v}}_k$ is UGAS. □

Proof (from Theorem 3.18, [6]): The proposed Lyapunov function candidate is

$$
V_3(\tilde{\boldsymbol{v}}_k, \tau_3) := e^{\lambda\tau_3} \sum_{k=1}^{N_3} c_3^k \tilde{\boldsymbol{v}}_k^\top \tilde{\boldsymbol{v}}_k \tag{12}
$$

where $\lambda > 0$ and $c_3 \in (0, 1)$ are constants. V_3 is lower and upper bounded by

$$
\alpha_1(\|\tilde{\boldsymbol{v}}_k\|) \leq V_3(\tilde{\boldsymbol{v}}_k, \tau_3) \leq \alpha_2(\|\tilde{\boldsymbol{v}}_k\|) \tag{13}
$$

where $\alpha_1(\|\tilde{\boldsymbol{v}}_k\|) := \sum_{k=1}^{N_3} c_3^k \tilde{\boldsymbol{v}}_k^\top \tilde{\boldsymbol{v}}_k$ and $\alpha_2(\|\tilde{\boldsymbol{v}}_k\|) := e^{\lambda\overline{T}_3} \sum_{k=1}^{N_3} c_3^k \tilde{\boldsymbol{v}}_k^\top \tilde{\boldsymbol{v}}_k$ are class κ_∞-functions.

The time derivative of V_3 along the trajectories of the velocity estimation error $\boldsymbol{f}_3(\tilde{\boldsymbol{v}}_k, \tau_3)$ is

$$
\begin{aligned}
\langle \nabla V_3(\tilde{\boldsymbol{v}}_k, \tau_3), \boldsymbol{f}_3 \rangle &= e^{\lambda\tau_3} \left(\lambda\dot{\tau}_3 \sum_{k=1}^{N_3} c_3^k \tilde{\boldsymbol{v}}_k^\top \tilde{\boldsymbol{v}}_k + 2 \sum_{k=1}^{N_3} c_3^k \tilde{\boldsymbol{v}}_k^\top \dot{\tilde{\boldsymbol{v}}}_k \right) \\
&= -\lambda V_3(\tilde{\boldsymbol{v}}_k, \tau_3).
\end{aligned}
$$

The difference in V_3 before and after a jump is upper bounded by

$$\begin{aligned} V_3(\tilde{\boldsymbol{v}}_k^+,\tau_3^+) - V_3(\tilde{\boldsymbol{v}}_k,\tau_3) \leq \\ e^{\lambda \overline{T}_3} \sum_{k=1}^{N_3} c_3^k \tilde{\boldsymbol{v}}_{k-1}^\top \tilde{\boldsymbol{v}}_{k-1} - \sum_{k=1}^{N_3} c_3^k \tilde{\boldsymbol{v}}_k^\top \tilde{\boldsymbol{v}}_k \\ = e^{\lambda \overline{T}_3} \sum_{k=2}^{N_3} c_3^k \tilde{\boldsymbol{v}}_{k-1}^\top \tilde{\boldsymbol{v}}_{k-1} - \sum_{k=1}^{N_3} c_3^k \tilde{\boldsymbol{v}}_k^\top \tilde{\boldsymbol{v}}_k. \end{aligned}$$

Here, we have contracted the first sum, as $\tilde{\boldsymbol{v}}_0 = \mathbf{0}$. Furthermore, we get

$$\begin{aligned} V_3(\tilde{\boldsymbol{v}}_k^+,\tau_3^+) - V_3(\tilde{\boldsymbol{v}}_k,\tau_3) \leq \\ e^{\lambda \overline{T}_3} \sum_{k=1}^{N_3-1} c_3^{k+1} \tilde{\boldsymbol{v}}_k^\top \tilde{\boldsymbol{v}}_k - \sum_{k=1}^{N_3} c_3^k \tilde{\boldsymbol{v}}_k^\top \tilde{\boldsymbol{v}}_k \\ \leq \sum_{k=1}^{N_3} [e^{\lambda \overline{T}_3} c_3^{k+1} - c_3^k] \tilde{\boldsymbol{v}}_k^\top \tilde{\boldsymbol{v}}_k. \end{aligned}$$

By choosing λ such that

$$c_3^k > e^{\lambda \overline{T}_3} c_3^{k+1} \;\Leftrightarrow\; \lambda < -\frac{\ln(c_3)}{\overline{T}_3}$$

the terms in the first sum will be dominated by the terms in the second sum. Thus, there exists a $\delta_3 > 0$ such that

$$V_3(\tilde{\boldsymbol{v}}_k^+, \tau_3^+) - V_3(\tilde{\boldsymbol{v}}_k, \tau_3) \leq -\delta_3 \tilde{\boldsymbol{v}}_k^\top \tilde{\boldsymbol{v}}_k. \tag{14}$$

Thus, V_3 satisfies the sufficient Lyapunov conditions, proving the velocity error dynamics in (10) UGAS (Theorem 3.18, [6]).

□

4.3 Position error analysis with zero input

We now analyze the position error dynamics in (11) under the assumption that the estimated velocity $\hat{\boldsymbol{v}}$ has converged to the real velocity $\boldsymbol{v}$, such that $\hat{\boldsymbol{v}} - \boldsymbol{v} = 0$. The position error dynamics are then given by the unforced system:

$$\begin{aligned} \dot{\tilde{\boldsymbol{\xi}}}_i &= \mathbf{0} && i \in \{1, ..., N_1\} \\ \tau_1 &= -1 \\ \tilde{\boldsymbol{\xi}}_i^+ &= \tilde{\boldsymbol{\xi}}_{i-1} && i \in \{1, ..., N_1\} \\ \tau_1^+ &\in [\underline{T}_1, \overline{T}_1] \end{aligned} \tag{15}$$

Note that these error dynamics have the same structure as the velocity error dynamics in (10).

Claim 2: Given that $\hat{\boldsymbol{v}} = \boldsymbol{v}$, the origin of the position observer error dynamics given by (15) is UGAS. □

Proof (from Theorem 3.18, [6]): The proposed Lyapunov function candidate is

$$V_1(\tilde{\boldsymbol{\xi}}_i, \tau_1) := e^{\mu\tau_1} \sum_{i=1}^{N_1} c_1^i \tilde{\boldsymbol{\xi}}_i^\top \tilde{\boldsymbol{\xi}}_i \tag{16}$$

where $\mu > 0$ and $c_1 \in (0, 1)$ are constants. V_1 is lower and upper bounded by

$$\alpha_3(\left\|\tilde{\boldsymbol{\xi}}_i\right\|) \leq V_1(\tilde{\boldsymbol{\xi}}_i, \tau_1) \leq \alpha_4(\left\|\tilde{\boldsymbol{\xi}}_i\right\|) \tag{17}$$

where $\alpha_3(\left\|\tilde{\boldsymbol{\xi}}_i\right\|) := \sum_{i=1}^{N_1} c_1^i \tilde{\boldsymbol{\xi}}_i^\top \tilde{\boldsymbol{\xi}}_i$ and $\alpha_4(\left\|\tilde{\boldsymbol{\xi}}_i\right\|) := e^{\mu \overline{T}_1} \sum_{i=1}^{N_1} c_1^i \tilde{\boldsymbol{\xi}}_i^\top \tilde{\boldsymbol{\xi}}_i$ are class κ_∞-functions.

The remainder of the proof follows the same procedure as the proof of Claim 1, and is due to space constraints excluded.

□

4.4 Position error analysis with non-zero input

We now relax the assumption that the estimated velocity has converged to the real velocity. We then have to take two considerations into account:

I) The velocity estimate may not be equal to the actual velocity, resulting in a non-zero input $\hat{\boldsymbol{v}} - \boldsymbol{v} \neq 0$ to the flow dynamics of the position error. This is captured in the dynamics of the first observer state, $\tilde{\boldsymbol{\xi}}_1$. In this case, we therefore restrict ourselves to the case where $N_1 = 1$.

II) The error in the position estimates introduced by the non-zero input $\hat{\boldsymbol{v}} - \boldsymbol{v}$ will propagate in the shift register when new measurements are obtained, such that $\tilde{\boldsymbol{\xi}}_{i-1} \neq 0$ for $i \in \{2, ..., N_1\}$ with $N_1 > 1$.

We analyze both cases subsequently.

4.4.1 Case I): Position error analysis with non-zero input for $N_1 = 1$

Recall that the dynamics of the position error with a non-zero input $\tilde{\boldsymbol{v}} \triangleq \hat{\boldsymbol{v}} - \boldsymbol{v}$ for the first observer state is given by

$$\begin{aligned} \dot{\tilde{\boldsymbol{\xi}}}_1 &= \boldsymbol{I}_{1:2} \boldsymbol{R}(\boldsymbol{\Theta}) \tilde{\boldsymbol{v}} \\ \tau_1 &= -1 \\ \tilde{\boldsymbol{\xi}}_1^+ &= \boldsymbol{0} \\ \tau_1^+ &\in [\underline{T}_1, \overline{T}_1] \end{aligned} \tag{18}$$

Claim 3: The system given by (18) with input $\tilde{\boldsymbol{v}} = \hat{\boldsymbol{v}} - \boldsymbol{v}$ is ISS. □

Proof (from Proposition 2.7, [11]): As shown in (17), V_1 is lower and upper bounded by two functions $\alpha_3(\left\|\tilde{\boldsymbol{\xi}}_i\right\|)$, $\alpha_4(\left\|\tilde{\boldsymbol{\xi}}_i\right\|) \in \kappa_\infty$. The time derivative of V_1 along the trajectories of the position estimation error $\boldsymbol{f}_1(\tilde{\boldsymbol{\xi}}_i, \tau_1)$ in the case where $N_1 = 1$ is

$$\begin{aligned}
\langle \nabla V_1(\tilde{\boldsymbol{\xi}}_i, \tau_1), \boldsymbol{f}_1 \rangle &= e^{\mu\tau_1} \left(\mu \dot{\tau}_1 c_1 \tilde{\boldsymbol{\xi}}_1^\top \tilde{\boldsymbol{\xi}}_1 + 2 c_1 \tilde{\boldsymbol{\xi}}_1^\top \dot{\tilde{\boldsymbol{\xi}}}_1 \right) \\
&= -\mu V_1(\tilde{\boldsymbol{\xi}}_i, \tau_1) + 2 c_1 e^{\mu\tau_1} \tilde{\boldsymbol{\xi}}_1^\top \boldsymbol{I}_{1:2} \boldsymbol{R}(\boldsymbol{\Theta}) \tilde{\boldsymbol{v}} \\
&\leq -\mu V_1(\tilde{\boldsymbol{\xi}}_i, \tau_1) + 2 c_1 e^{\mu\tau_1} \left\| \tilde{\boldsymbol{\xi}}_1^\top \boldsymbol{I}_{1:2} \boldsymbol{R}(\boldsymbol{\Theta}) \tilde{\boldsymbol{v}} \right\| \\
&\leq -\mu V_1(\tilde{\boldsymbol{\xi}}_i, \tau_1) + 2 c_1 e^{\mu\tau_1} \left\| \tilde{\boldsymbol{\xi}}_1^\top \right\| \left\| \boldsymbol{I}_{1:2} \right\| \left\| \boldsymbol{R}(\boldsymbol{\Theta}) \tilde{\boldsymbol{v}} \right\| .
\end{aligned}$$

Here, we have used that $\tilde{\boldsymbol{\xi}}_1^\top \boldsymbol{I}_{1:2} \boldsymbol{R}(\boldsymbol{\Theta}) \tilde{\boldsymbol{v}} \leq \left\| \tilde{\boldsymbol{\xi}}_1^\top \boldsymbol{I}_{1:2} \boldsymbol{R}(\boldsymbol{\Theta}) \tilde{\boldsymbol{v}} \right\|$ and $\left\| \tilde{\boldsymbol{\xi}}_1^\top \boldsymbol{I}_{1:2} \boldsymbol{R}(\boldsymbol{\Theta}) \tilde{\boldsymbol{v}} \right\| \leq \left\| \tilde{\boldsymbol{\xi}}_1^\top \right\| \left\| \boldsymbol{I}_{1:2} \right\| \left\| \boldsymbol{R}(\boldsymbol{\Theta}) \tilde{\boldsymbol{v}} \right\|$, where $\|\cdot\|$ denotes the Euclidean norm. By using that $\left\| \boldsymbol{R}(\boldsymbol{\Theta}) \tilde{\boldsymbol{v}} \right\| = \left\| \tilde{\boldsymbol{v}} \right\|$ and $\left\| \boldsymbol{I}_{1:2} \right\| = \sqrt{2}$, we get

$$\begin{aligned}
\langle \nabla V_1(\tilde{\boldsymbol{\xi}}_i, \tau_1), \boldsymbol{f}_1 \rangle \leq & -\mu V_1(\tilde{\boldsymbol{\xi}}_i, \tau_1) \\
& + 2\sqrt{2} c_1 e^{\mu\tau_1} \left\| \tilde{\boldsymbol{\xi}}_1^\top \right\| \left\| \tilde{\boldsymbol{v}} \right\| .
\end{aligned}$$

By adding and subtracting the term $\sigma\mu \exp(\mu\tau_1) c_1 \left\| \tilde{\boldsymbol{\xi}}_1 \right\|^2$, where $\sigma \in (0, 1)$ is a constant, we get

$$\begin{aligned}
\langle \nabla V_1(\tilde{\boldsymbol{\xi}}_i, \tau_1), \boldsymbol{f}_1 \rangle \leq & -\mu(1-\sigma) V_1(\tilde{\boldsymbol{\xi}}_i, \tau_1) \\
& + 2\sqrt{2} c_1 e^{\mu\tau_1} \left\| \tilde{\boldsymbol{\xi}}_1^\top \right\| \left\| \tilde{\boldsymbol{v}} \right\| \\
& - \sigma\mu e^{\mu\tau_1} c_1 \left\| \tilde{\boldsymbol{\xi}}_1 \right\|^2 .
\end{aligned}$$

Finally, this is upper bounded by

$$\langle \nabla V_1(\tilde{\boldsymbol{\xi}}_i, \tau_1), \boldsymbol{f}_1 \rangle \leq -\mu(1-\sigma) V_1(\tilde{\boldsymbol{\xi}}_i, \tau_1)$$

for

$$\left\| \tilde{\boldsymbol{\xi}}_1 \right\| \geq \frac{2\sqrt{2}}{\sigma\mu} \left\| \tilde{\boldsymbol{v}} \right\| = \boldsymbol{\rho}(\left\| \tilde{\boldsymbol{v}} \right\|) \tag{19}$$

where $\boldsymbol{\rho}$ is a class κ-function. Under the assumption that $(\boldsymbol{\xi}, z, \boldsymbol{v}) \in \mathcal{K} \subset \mathbb{R}^6$, the input $\tilde{\boldsymbol{v}}$ will be bounded. It follows that $V_1(\tilde{\boldsymbol{\xi}}_i, \tau_1)$ is an ISS-Lyapunov function for (18), and thus the system (18) is ISS with respect to input $\tilde{\boldsymbol{v}} = \hat{\boldsymbol{v}} - \boldsymbol{v}$ (Proposition 2.7, [11]).

□

Theorem 2: The origin of the cascaded system consisting of the position error dynamics in (18) and the velocity error dynamics in (10) is UGAS. □

Proof (from Corollary 19, [10]): Consider the hybrid system $\mathcal{H} = (C, \boldsymbol{F}, D, \boldsymbol{G})$ consisting of the position error dynamics in (18) and the velocity error dynamics in (10). The compact set

$$\begin{aligned}\hat{\mathcal{A}} := \{(\boldsymbol{\xi}, \boldsymbol{v}), (\boldsymbol{\xi}_i, \boldsymbol{v}_k), (\tau_1, \tau_3) \in C : \boldsymbol{\xi}_i = \beta\mathbb{B},\, \boldsymbol{v}_k = \boldsymbol{v},\\ \forall i \in \{1, ..., N_1\}\, \forall k \in \{1, ..., N_3\}\}\end{aligned} \tag{20}$$

where $\beta > 0$ and $\mathbb{B}$ is the unit ball, is globally pre-asymptotically stable (GpAS) for $\mathcal{H}$ (Claim 1). Further, the compact set $\mathcal{A} \subset \hat{\mathcal{A}}$ from (7) is GpAS for $\mathcal{H}|_{\hat{\mathcal{A}}} := (C \cap \hat{\mathcal{A}}, \boldsymbol{F}, D \cap \mathcal{A}_1, \boldsymbol{G} \cap \hat{\mathcal{A}})$ (Claim 2). Then, the set $\mathcal{A}$ is UGAS for $\mathcal{H}$, given by the position and velocity error dynamics (18) and (10) (Corollary 19, [10]). □

4.4.2 Case II): Position error analysis with non-zero input for $N_1 > 1$

Now, we consider the case where we treat $\tilde{\boldsymbol{\xi}}_{i-1} \neq 0$ for $i \in \{2, ..., N_1\}$ as the input. Recall that the position error dynamics in this case are given by:

$$\begin{aligned}\dot{\tilde{\boldsymbol{\xi}}}_i &= \boldsymbol{0} && i \in \{2, ..., N_1\}\\ \dot{\tau}_1 &= -1 &&\\ \tilde{\boldsymbol{\xi}}_i^+ &= \tilde{\boldsymbol{\xi}}_{i-1} && i \in \{2, ..., N_1\}\\ \tau_1^+ &\in [\underline{T}_1, \overline{T}_1] &&\end{aligned} \tag{21}$$

The case when $N_1 = 1$ was analyzed in Case II) in order to capture the dynamics of the first observer state. Therefore, for $N_1 > 1$, we only need to consider $i \in \{2, ..., N_1\}$. Here, the flow dynamics will be the same as in the unforced position error dynamics in (15). However, there will be a non-zero input in the jump dynamics.

Claim 4: The system given by (21) with input $\tilde{\boldsymbol{\xi}}_{i-1}$ is ISS. □

Proof (from Proposition 2.7, [11]): The flow dynamics are unchanged. The change in V_1 before and after a jump is

$$\begin{aligned}V_1(\tilde{\boldsymbol{\xi}}_i^+, \tau_1^+) - V_1(\tilde{\boldsymbol{\xi}}_i, \tau_1) &\leq e^{\mu\overline{T}_1} \sum_{i=1}^{N_1} c_1^i \tilde{\boldsymbol{\xi}}_{i-1}^\top \tilde{\boldsymbol{\xi}}_{i-1} - \sum_{i=1}^{N_1} c_1^i \tilde{\boldsymbol{\xi}}_i^\top \tilde{\boldsymbol{\xi}}_i\\ &= -\alpha_5(\left\|\tilde{\boldsymbol{\xi}}_i\right\|) + \alpha_6(\left\|\tilde{\boldsymbol{\xi}}_{i-1}\right\|)\end{aligned}$$

where $\alpha_5(\left\|\tilde{\boldsymbol{\xi}}_i\right\|) := \sum_{i=1}^{N_1} c_1^i \tilde{\boldsymbol{\xi}}_i^\top \tilde{\boldsymbol{\xi}}_i$ is a class κ_∞-function and $\alpha_6(\left\|\tilde{\boldsymbol{\xi}}_{i-1}\right\|) := \exp(\mu\overline{T}_1) \sum_{i=1}^{N_1} c_1^i \tilde{\boldsymbol{\xi}}_{i-1}^\top \tilde{\boldsymbol{\xi}}_{i-1}$ is a class κ-function. Under the assumption that $(\boldsymbol{\xi}, z, \boldsymbol{v}) \in \mathcal{K} \subset \mathbb{R}^6$, the input $\tilde{\boldsymbol{\xi}}_{i-1}$ will be bounded. It follows that $V_1(\tilde{\boldsymbol{\xi}}_i, \tau_1)$ is an ISS-Lyapunov function for (21), and thus the system (21) is ISS with respect to input $\tilde{\boldsymbol{\xi}}_{i-1}$ (Proposition 2.7, [11]). □

Theorem 3: The origin of the cascaded system consisting of the position error dynamics in (21) and the velocity error dynamics in (10) is UGAS. □

The proof of Theorem 3 follows the same procedure as the proof of Theorem 2, and is due to space constraints excluded. □

4.5 Depth error analysis

Note that the depth error dynamics and the position error dynamics in (11) have the same structure.

Theorem 4: The origin of the cascaded system consisting of the depth error dynamics in (11) and the velocity error dynamics in (10) is UGAS. □

The proof of Theorem 4 follows the same procedure as the proof of Theorem 3, and is due to space constraints excluded. □

4.6 Stability of total observer

We have now established that the origin of the cascaded system consisting of the position observer and the velocity observer with a non-zero velocity estimation error is UGAS (Theorem 2 and 3). Furthermore, we have established that the origin of the cascaded system consisting of the depth observer and the velocity observer with a non-zero velocity estimation error is UGAS (Theorem 4). Using the fact that the position error dynamics and the depth error dynamics are independent of each other, the set $\mathcal{A}$ in (7) is UGAS for all $i \in \{1, ..., N_1\}$, $j \in \{1, ..., N_2\}$ and $k \in \{1, ..., N_3\}$ for the velocity observer in (10) in cascade with the position and depth observers in (11). This concludes the proof of Theorem 1.

□

5 Simulation results and discussion

This Section presents the setup of the simulations and discussions of the results.

5.1 Case study

As a case study, an under-ice operation of an autonomous underwater vehicle (AUV) is used. The observer is simulated in closed-loop with a control system where the objective is to follow a lawnmower trajectory in the horizontal plane, while maintaining a constant distance of 10 meters to the ice surface. In this case study, the sensor measurements have a high level of sporadicity, that is, large maximum sampling periods, in order to simulate sensors in bad condition.

5.2 Simulation setup

The observer was implemented in MATLAB/Simulink using the Hybrid Equations Toolbox v2.04 [12]. The simulator used is an Arctic AUV simulator created by Norgren [13] in MATLAB/Simulink and C++.

The numerical values of the observer parameters are given in Table 1.

Noise with standard deviations $\sigma_{imu} = 0.007$ $[m/s^2]$, $\sigma_1 = 0.5$ $[m]$, $\sigma_2 = 0.001$ $[m]$ and $\sigma_3 = 0.003$ $[m/s]$ were added on the IMU, acoustic positioning system, pressure gauge and DVL measurements, respectively. All observer states are initialized with the first measurements.

		Observer type		
		Position ($m = 1$)	Depth ($m = 2$)	Velocity ($m = 3$)
N_m	[-]	40	10	15
γ_m	[-]	1.0	0.75	0.8
$\underline{T}_m$	[s]	0.5	0.125	0.2
$\overline{T}_m$	[s]	5	1.250	2.0

Table 1: Numerical values of observer parameters.

5.3 Sensitivity analysis on observer parameters

A sensitivity analysis on the observer parameters was conducted in [5]. Here, open-loop motions were simulated for different values of the number of states N_1, N_2 and N_3 and the discount factors γ_1, γ_2 and γ_3. The results showed that the value of these parameters should be tuned in accordance with the relative uncertainty in the sensor measurements governing the flow dynamics and the jump dynamics, respectively.

The observer was also simulated for different maximum sampling rates $\overline{T}_m$ and different levels of noise σ_{imu} on the acceleration measurements. The results showed that the observer was robust with respect to these parameters.

5.4 Simulation results and discussions

Figure 3 shows the simulated trajectory of the AUV under the sea ice. Figure 4 shows the estimation errors of the observer. As seen, the observer successfully estimates the linear positions and velocities with acceptable estimation errors. The control system also performs well in closed-loop with the observer.

This hybrid observer concept is not reliant on any complicated mathematical operations and does not require much memory. Therefore, in most practical contexts, computational complexity will not be a challenge.

Here, we have assumed that the acceleration measurements are continuously available. When implementing this observer in a computer, one must make sure that the sampling rate of the IMU is considerably faster than the position, depth and velocity measurements. This will not be a problem in most cases.

It is expected that this observer concept is sensitive to the accuracy of the attitude estimation. For future work, the observer performance should therefore be evaluated in closed-loop with an attitude observer. Establishing certain robustness and recurrence properties when taking into account the effect of noise in the measurements, as well as errors in the attitude estimation, is also of interest.

Note that there is a transient time after initialization of the observer. This is because the observer needs time to obtain the required number of measurements. After this, the observer will not have any transients.

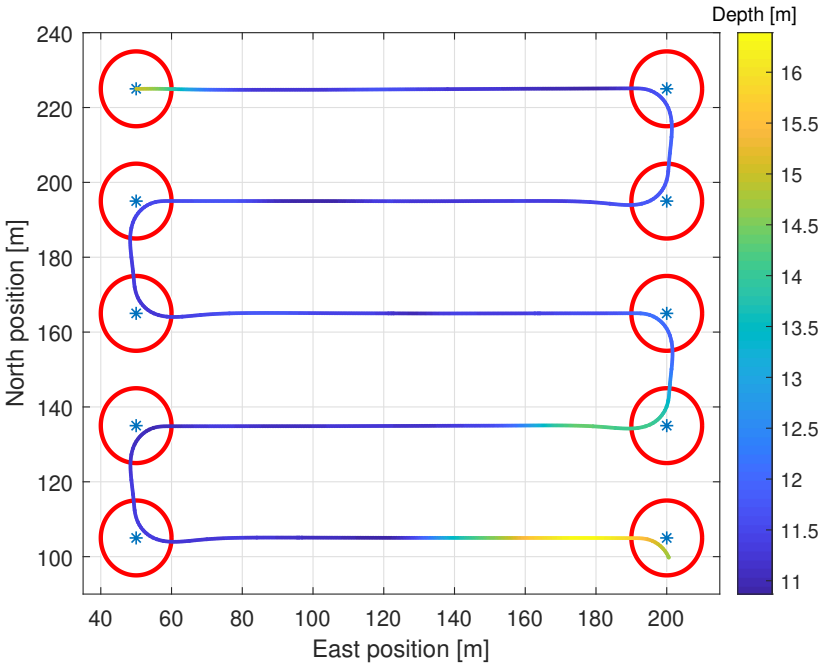

Figure 3: North-East trajectory of the AUV with a color plot showing the depth. The blue stars denote waypoints with red circles of acceptance.

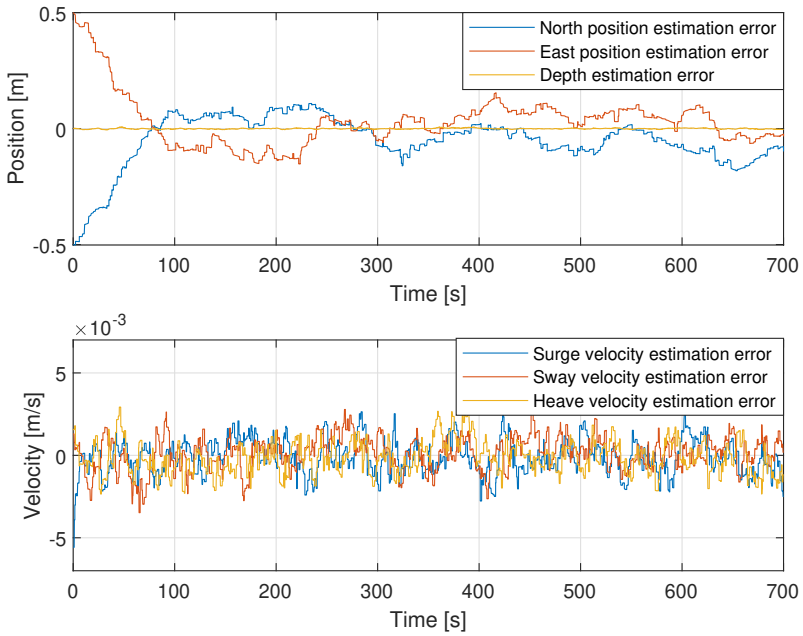

Figure 4: Observer estimation errors in position and velocity.

6 Conclusions

The proposed sensor-based hybrid translational observer performed well in the simulations, and UGAS was established using Lyapunov theory for hybrid and cascaded systems. The performance depends on the choice of the number of states N_1, N_2 and N_3 and the discount factors γ_1, γ_2 and γ_3 in the position, depth and velocity observers, respectively. The value of these parameters should be tuned according to the relative uncertainty in the measurements governing the jump dynamics and the flow dynamics.

References

[1] K. Gade, "Inertial navigation — theory and applications," PhD thesis 2018:38, Dept. of Engineering Cybernetics, Faculty of Information Technology and Electrical Engineering, NTNU, Trondheim, 2018.

[2] D. Steinke and B. Buckham, "A Kalman filter for the navigation of remotely operated vehicles," in *Proc. of OCEANS 2005 MTS/IEEE*, vol. 1, Washington, D.C., pp. 581–588, 2005.

[3] J. E. Refsnes, A. J. Sørensen, and K. Y. Pettersen, "Model-based output feedback control of slender-body underactuated AUVs: Theory and exper-

iments," *IEEE Transactions on Control Systems Technology*, vol. 16, no. 5, pp. 930–946, 2008.

[4] F. Dukan, "ROV motion control systems," PhD thesis 2014:295, Department of Marine Technology, Faculty of Engineering, NTNU, Trondheim, 2014.

[5] J. E. Bremnes, A. H. Brodtkorb, and A. J. Sørensen, "Sensor-based hybrid translational observer for underwater navigation," in *Proc. of the 12th IFAC Conference on Control Applications in Marine Systems, Robotics and Vehicles*, Daejeon, pp. 378–383, 2019.

[6] R. Goebel, R. G. Salfelice, and A. R. Teel, "Hybrid dynamical systems : Modeling, stability, and robustness." Princeton, 2012.

[7] A. H. Brodtkorb, A. R. Teel, and A. J. Sørensen, "Sensor-based hybrid observer for dynamic positioning," in *Proc. of the 54th IEEE Conference on Decision and Control*, Osaka, pp. 948–953, 2015.

[8] M. Ludvigsen and A. J. Sørensen, "Towards integrated autonomous underwater operations for ocean mapping and monitoring," *Annual Reviews in Control*, vol. 42, pp. 145–157, 2016.

[9] A. J. Sørensen, "Marine control systems : Propulsion and motion control of ships and ocean structures," Department of Marine Technology, Faculty of Engineering, NTNU, Trondheim, 2013.

[10] R. Goebel, R. G. Sanfelice, and A. R. Teel, "Hybrid dynamical systems," *IEEE Control Systems*, vol. 29, no. 2, pp. 28–93, 2009.

[11] C. Cai and A. R. Teel, "Characterizations of input-to-state stability for hybrid systems," *Systems & Control Letters*, vol. 58, no. 1, pp. 47–53, 2009.

[12] R. Sanfelice, D. Copp, and P. Nanez, "A toolbox for simulation of hybrid systems in matlab/simulink: Hybrid equations (hyeq) toolbox," in *Proc. of the 16th ACM Int. Conference on Hybrid Systems: Computation and Control*, New York, pp. 101–106, 2013.

[13] P. Norgren, "Autonomous underwater vehicles in arctic marine operations: Arctic marine research and ice monitoring," PhD thesis 2018:255, Dept. of Marine Technology, Faculty of Engineering, NTNU, Trondheim, 2018.